

Dear editor,

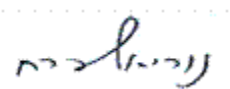
We thank you for the positive feedback on our paper and for the opportunity to revise our manuscript following the constructive suggestions of both reviewers. We accepted all of their comments as described in details below. Please note that line numbers refer to the final PDF revised paper.

The main changes in the revised manuscript include:

- 1) We changed discussion on the minor differences between previous and new ID data which are indeed largely overlapping within uncertainties.
- 2) We included footnotes for all supplementary tables (S1-S8)
- 3) We included some new LA-MC-ICPMS data from 2018-2020 in Fig. 4b and Table S5.
- 4) We included new figure 8 and section 4.5 dedicated to discussion on U-Pb concentrations of available standards and comparison to concentrations in carbonate material.

Sincerely,

Perach Nuriel, on behalf of all co-authors



Dr. Perach Nuriel

The Geological Survey of Israel

32 Yeshayahu Leibowitz St. Jerusalem, 9692100, Israel

Email: nuriel@gsi.gov.il

Tel: 972-2-5314207

Reviewer answer letter

“The use of ASH-15 flowstone as a matrix-matched reference material for laser-ablation U-Pb geochronology of calcite”

AC1

Fernando Corfu (Referee)

fernando.corfu@geo.uio.no

Received and published: 14 August 2020

The paper reports the results of a calibration of carbonate to be used as reference material. Measurements were done with various ICP instruments and operators, and by two ID-TIMS laboratories. The data are good and important, considering the type of material and the very young age of the samples, and considering the purpose of the study. I find the fundamental elements of the paper to be correct. At the same time, some of the terms used and descriptions of the material and sample targets are confusing and I recommend that the authors consider using better terms and correct some of the confusing parts.

We greatly appreciate the reviewer's comments and good suggestions that helped to improve this contribution. Please see our specific answers to each comment.

Comment: There is a terms 'growth bands' which I first assumed to mean growth zones (line in an onion) only to find out that it designated zones perpendicular to growth zones. Then there are two transects for ICP spot analyses, the two being perpendicular to each other. Even enlarging Fig. 2 I can only see a row of spots, so I cannot really understand where the layer-parallel transect would be. Eventually after reading to the end one gets the idea, but it would simplify matters if the text and figures would not create confusion in the first place.

Answer: We agree and we corrected this confusing terms to 'spots array along growth zone' and 'along growth direction'. We also improve Figure 2 with a new XPL image showing nicely growth direction and a new close-up image of the two spot arrays.

Comment: I have made some suggestions and comments in the text.

Answer: all suggestions are corrected in the revised paper, many thanks for thorough reading.

Comment: The data are reported in sheets of an excel file, which is fine. The ID-TIMS data are given in great detail, and have good footnotes explaining the nature of all the entries. By contrast the ICP tables have essentially no explanations. They seem to be working table just thrown in without bothering to format them properly, explaining what the data mean and how/where they were treated and produced. I suppose this is all evident for the authors. The readers do not count? Please make sure the tables are well prepared and informative.

Answer: We included footnotes in all tables in the supplementary file (S1-S8).

AC2

Jon Woodhead (Referee)

jdwood@unimelb.edu.au

Received and published: 28 August 2020

Comment: The in-situ carbonate U-Pb chronometer is an exciting development finding a host of new applications across a range of Geoscience disciplines. The main impediment to its use remains the dearth of suitable (moderate U, Pb, homogeneous) calcites that can be utilised as reference materials. Most practitioners are now using the WC-1 calcite (Roberts et al) as a primary calibrant and employing analytical strategies to compensate for its non-homogeneous characteristics but there remains an urgent need for the development of further reference materials. This manuscript takes a step along this path providing accurate ID data for the ASH-15 speleothem material which is used by many labs as a secondary standard.

The analytical procedures documented in the manuscript appear rigorous and the close correspondence between data from different laboratories is very encouraging. Notably the scatter about the ASH-15 isochron is considerably less than that observed for WC-1 suggesting that ASH-15 could be adopted as a primary calibrant, offering more precise age determinations. As such I think this is a valuable contribution to Geochronology and should be published with minor modifications.

Answer: We greatly appreciate the reviewer's comments and good suggestions that helped to improve this contribution. Please see our specific answers to each comment.

Comment: my main concern with the manuscript stems from the comparison with previous ID determinations for the ASH-15 material (primarily Vaks et al., 2013, Mason et al., 2013, although see later discussion). At the outset (line 35) the authors note that the new ID-TIMS ages are '1.3-1.5% younger than previously suggested' and later (lines 388 onwards) in the

manuscript there is considerable discussion surrounding an observation that the literature ages are 'systematically older' and that the 'origin of this bias should be investigated'. In fact (as the authors themselves note) the new and literature ages for the individual determinations by each lab are all within uncertainty of each other and so, as far as I can see, they must therefore be statistically indistinguishable? Once the grand mean for the current study is employed the overlap in uncertainties is admittedly minor but, at that point, any statistical comparison is invalidated because data from two different labs have already been combined.

Answer: Indeed there is overlap within uncertainties and we have revised the text as suggested (lines 388-391):

"These ages are largely overlapping within uncertainty with our new ID-TIMS age of 2.965 ± 0.011 Ma (Fig. 7; and data in Table S7 in the supplements). The apparent minor systematic offset towards slightly older ages is attributed to the lower number of aliquots in the MC-ICPMS datasets combined with the heterogeneous initial Pb isotope composition."

Comment: In addition, no mention is made of the University of Leeds determination (Vaks et al, Supplementary table 3) which is from yet another lab and is also in agreement with all of these numbers.

Answer: Unfortunately, we forgot to point on the data from the University of Leeds in Figure 7 (although shown on the RHS). We have now revised Figure 7 to indicate in which lab each date was obtained.

Comment: So, as far as I can see, the existing data from 5 different labs - all using slightly different analytical approaches - are all statistically identical? No biases required. Of course a case can be mounted that the new data are based on more aliquots and therefore may be more robust (in terms of common Pb intercept, for example) but I do not see any justification for looking for a bias here when, in fact, the statistics tell us that there is very little evidence of such. I think that it would be far more honest to simply say that the new data are 'statistically indistinguishable from the literature values but considerably more precise'.

Answer: We accept this comment and we revised this part as suggested (see lines 388-391 above).

A few more minor points:

Comment: 1. Lines 320, 329 what is the justification for the common Pb anchor of 0.8315? The TIMS data seem to show intercepts ranging from 0.814 to 0.832 and all show minor heterogeneity in 207/206 initial. Is this value a weighted mean of the ID TIMS data?

Comment: 2. Also, it might be worth processing LA data with slightly different value – that might explain the slightly younger age of the LA data cf TIMS?

Answer: To avoid changing the common-lead value for each TW plot we did not use anchoring in age calculations in the revision.

Comment: 3. Re. the discussion at lines 383-393 alluded to above:

Why were ages the literature recalculated? Is this due to differences in error handling between Isoplot and Isoplot-R?

Answer: Indeed. We wanted to calculate all the data with the exact same settings: same decay constant, with the same anchoring or no anchoring, without disequilibrium correction and without propagating external uncertainties.

Comment: Figure 7 shows two different fields for 'ASH15D (Vaks et al)' which are quite different. What is the lower one (RHS), not mentioned in the text?

Answer: This is the missing data from Leeds lab, we now indicate it in the revised Figure 7.

Comment: The use of EarthTime reference materials (line 396) is not unique to the current study as suggested here and this argument should not be used in an attempt to cast doubts on the literature data. The Supplementary information for Vaks et al. (2013) clearly states 'sample solutions were spiked, using a 233U-205Pb tracer, calibrated against EarthTime U-Pb normals'. Similarly (lines 397-398), although double spiking may well be important for control of mass bias effects in TIMS, the relatively stable mass bias of plasma instruments means that the bias correction is actually a very small component of the uncertainty budget for ID-MCICPMS. As noted above the main advantage of the current study is undeniably the larger number of analyses contributing to lower uncertainty. I think that most of the other arguments posited in lines 389-398 are probably illusory.

Answer: We removed 'compared to previous bulk analyses' from this sentence.

Comment: Lines 24, 354 etc refer to 'high precision ID TIMS'. I may be mistaken but I don't think that there is really such a thing these days as 'low precision ID TIMS' (!) so the words 'high precision' are unnecessary hyperbole.

Answer: We removed 'high-precision' from these lines.

Comment: Line 185 to what does the term 'dosage' refer? Is this something specific to the ARIS laser sample introduction system?

Answer: We added a short explanation after the word 'dosage' in the text in line 186-187:
“(10 overlapping pulses per spot size which amount to a scanning speed of 588 μms^{-1})”

Comment: Finally, I think that the manuscript would benefit from some discussion of the relative merits of an ideal calcite reference material. While extreme homogeneity seems an almost impossible goal, there are also clearly 'sweet spots' for both U and Pb content when using different instruments/analysing different samples and it would be beneficial to explore this trade-off here – as an aid to the general reader. ASH15 appears to have about half the U content of WC-1 but it also has very low Pb content requiring relatively large spot sizes compared to WC-1. This is alluded to in the last line of the conclusions, but it would be nice to see both WC-1 and ASH-15 plotted relative to the range of calcites commonly encountered e.g. by using the plots from Roberts et al 2020 (Geochronology) Fig 5. Then we can visually determine how well suited they are as standards for the analysis of such materials and indeed where we should be looking for the next standard (in terms of U and Pb content).

Answer: We thank the reviewer for this suggestion and we added in the revised manuscript figure (Figure 8) that shows concentrations comparison of WC1, ASH15 and JT reference materials as well as different carbonate material. We also included a whole section (4.5, lines 410-431) that elaborate on these issues:

“4.5. Calcite reference material

The U and Pb concentrations of carbonate materials vary greatly. Data compilation by Roberts et al. (2020; this issue) combined hundreds of carbonate samples from different origin such as diagenetic, biogenic, speleothem, and vein-fill. This compilation indicates several orders of magnitude differences in U and Pb concentrations of the different types of carbonate and the heterogeneity of spot analysis within each type or even a single sample. A modified representation of their data, excluding calcite vein-fill, which vary throughout the entire compositional range, is shown together with the currently available calcite reference materials (Fig. 8; and full data in Table S8 in the supplement). Note that both ASH15 and JT, display much

larger heterogeneity when measured by LA-ICPMS (small symbols) relative to ID-TIMS (large symbols). Despite the high compositional heterogeneity of each of the reference material, they show minimal overlap and together they cover most of the compositional range of the presented carbonate material. WC1 (Roberts et al., 2017) with relatively high U and Pb concentrations can easily be measured on single collector ICPMS (including quadrupole instruments) and is most appropriate to be used for dating vein-fill and diagenetic carbonates. In contrast, the ASH15 flowstone, with relatively low Pb and high U concentration that are better measured on sector-field (MC)-ICPMS is most appropriate for dating speleothem type carbonates. Finally the JT (Guillong et al., 2020), with moderate U and Pb concentration can be used on both single- and multi-collector sector field ICPMS instruments and for all types of carbonate samples. Reference material with high Pb and low U or both low U and Pb concentrations will further help to cover the full compositional range of carbonate material but may introduce analytical challenges.”

1 **The use of ASH-15 flowstone as a matrix-matched reference material for laser-ablation**
2 **U-Pb geochronology of calcite**

3 Perach Nuriel¹, Jörn-Frederik Wotzlaw², Maria Ovtcharova³, Anton Vaks¹, Ciprian Stremtan⁴,
4 Martin Šala⁵, Nick M. W. Roberts⁶, and Andrew R. C. Kylander-Clark⁷

5

6 ¹ Geological Survey of Israel, 32 Yeshayahu Leibowitz St. Jerusalem, 9692100, Israel

7 ² Institute of Geochemistry and Petrology, ETH Zurich, Clausiusstrasse 25 I CH-8092 Zurich,
8 Switzerland

9 ³ Department of Earth Sciences, University of Geneva, Geneva, Switzerland

10 ⁴ Teledyne Photon Machines, 384 Gallatin Park Drive, Bozeman, MT 59715, USA

11 ⁵ Department of Analytical Chemistry, National Institute of Chemistry, Hajdrihova 19, SI-1000
12 Ljubljana, Slovenia.

13 ⁶ Geochronology and Tracers Facility, British Geological Survey, Environmental Science
14 Centre, Nottingham, NG12 5GG, UK

15 ⁷ Department of Earth Science, University of California, Santa Barbara, CA 93106, USA.

16

17 **Abstract**

18 Latest advances in laser ablation inductively coupled plasma mass spectrometer (LA-ICPMS)
19 allow for accurate *in-situ* U-Pb dating of carbonate material, with final age uncertainties usually
20 >3% 2 σ . Cross-laboratory reference materials (RMs) used for sample-bracketing are currently
21 limited to WC1 calcite with an age of 254.4 ± 6.5 (2 σ). The minimum uncertainty on any age
22 determination with the LA-ICPMS method is therefore $\geq 2.5\%$, and validation by secondary
23 RMs ~~are~~is usually performed on in-house standards. This contribution present a new reference
24 material, ASH-15, a flowstone that is dated here by isotope dilution (ID) TIMS analysis
25 using ~~36-37~~ sub-samples, 1-7 mg each. Age results presented here are slightly younger

26 compared to previous ID-IRMS U-Pb ~~dating dates~~ of ASH-15, but within uncertainties and in
27 agreement with *in-situ* analyses (using WC1 as the primary RM). We provide new correction
28 parameters to be used as primary or secondary standardization. The suggested $^{238}\text{U}/^{206}\text{Pb}$
29 apparent age, not corrected for disequilibrium and without common-lead anchoring, is $2.965 \pm$
30 0.011 Ma (2σ). The new results could improve the propagated uncertainties on the final age
31 with a minimal value of 0.4%, which is approaching the uncertainty of typical ID analysis on
32 higher-U materials, for example, such as zircon (<1% 2s). We show that although LA-ICPMS
33 spot analyses of ASH-15 exhibit significant scatter in their isotopic ratios, the down-hole
34 fractionation of ASH-15 is similar to that of other reference materials. This high-U (~1 ppm)
35 and low Pb (<0.01 ppm) calcite is most appropriate as a reference material for other
36 speleothem-type carbonates but requires sensitive sector-field ICP-MS instruments. Reference
37 materials with high Pb and low U or both low U and Pb compositions are still needed to fully
38 cover the compositional range of carbonate material but may introduce analytical challenges.
39 ~~For LA work, we recommend the use of the new ID-TIMS ages that are 1.3–1.5% younger than~~
40 ~~previously suggested, because of the lower uncertainties (0.4%), the large number of sub-~~
41 ~~samples (n=36), the use of the EARTHTIME isotopic tracers, and the small aliquots (1–7 mg)~~
42 ~~that are more representative of laser-ablation spot analysis.~~

43

44 **Introduction**

45 Recent advances in laser ablation techniques applied to multi-phase carbonates allow for
46 accurate dating of a variety of sample types, including calcite cements (Li et al., 2014; Godeau
47 et al., 2018; Anjiang et al., 2019; Holdsworth et al., 2019), hydrothermal veins (Coogan et al.,
48 2016; MacDonald et al., 2019; Piccione et al., 2019), fault-related veins, breccia cement, and
49 slickenfibers (Ring and Gerdes, 2016; Roberts and Walker, 2016; Goodfellow et al., 2017;

50 Nuriel et al., 2017; Hansman et al., 2018; Parrish et al., 2018; Nuriel et al., 2019), and
51 speleothems (Woodhead and Petrus, 2019). With increasing attention ~~on~~to climatic, seismic,
52 and environmental events in the geological record, there is a growing need for dating
53 techniques that can be accurately and easily implemented ~~to~~for samples at the sub-millimeter
54 scale. This newly emerging technique has the potential to contribute to our understanding of
55 the duration, rate, and extent of these important events in the geological record.

56 The *in-situ* approach has a great research potential for studying texturally complex samples
57 because it can resolve problems of age mixing of different phases or averaging of continuous
58 growth at the sub-millimeter scale, and thus increase the overall accuracy of the dated material.
59 While the precision of traditional isotope-dilution (ID) U-Pb analyses is still favorable (<1%
60 2σ) (Woodhead and Petrus, 2019), the increasing analytical development of the LA-ICPMS
61 method indicates the potential for improving the currently reported uncertainties (usually >3%
62 2σ). Finding the right matrix-matched reference material (RM) is a major hurdle for LA
63 analyses of carbonates because of the variety of mineralogy (calcite, dolomite, and aragonite),
64 textures, composition (e.g. high-magnesium calcite, high common-lead), and ages (e.g. low
65 radiogenic lead in young samples). Textural differences such as microcrystalline, fine- and
66 coarse-grained material, between the unknown and RMs can contribute to high uncertainties
67 due to differences in ablation efficiency, down-hole fractionation, and differences in crater
68 morphology (e.g. Guillong et al., 2020 and Elisha et al, 2020, this issue). Observed deviations
69 are potentially up to 20% of the final intercept age depending on the degree of crater geometry
70 mismatch and are related ~~to~~ either to downhole fractionation and/or matrix effects (Guillong
71 et al., 2020).

72 Currently, the most commonly used procedure for mass-bias correction in the LA method, is
73 by standard-sample bracketing. For this, the $^{238}\text{U}/^{206}\text{Pb}$ LA-age of the RMs is corrected to the
74 true RM's $^{238}\text{U}/^{206}\text{Pb}$ apparent age (not corrected for disequilibrium) as measured

75 independently by an ID-IRMS method (e.g. ID-TIMS or ID-MC-ICPMS). The RMs are
76 measured throughout each session along with the unknown samples, and a normalization factor
77 is applied to correct both the RMs and the unknowns. Uncertainty propagation onto the age of
78 the unknowns includes the uncertainties of the ‘true’ RM age. As a result, the accuracy of the
79 LA analyses can only be as good as the uncertainties on the age of the RMs which is by itself
80 subjected to analytical challenges due to natural heterogeneities, impurities, and textural
81 complexities at the sub-millimetre scale. It is therefore essential that the ‘true age’ of the
82 reference material will reflect these complexities while maintaining minimal uncertainties.

83 Currently, several in-house standards are being used as reference materials, including Duff
84 Brown Tank (64 Ma; Hill et al., 2016), and JT (13.797 ± 0.031 Ma; Guillong et al., 2020). The
85 only well-characterized reference material that is distributed across laboratories is the WC1
86 calcite with an age of 254.4 ± 6.5 2s (2.5%) (Roberts et al., 2017). The use of WC1 alone for
87 mass-bias correction has several disadvantages. First, it is highly recommended with all in situ
88 U-Th-Pb geochronology to use secondary RMs to validate any correction parameters that are
89 being used, and to appropriately propagate uncertainties. Second, the relatively high
90 uncertainty (2.5%) on the age of WC1 sets a minimal uncertainty on any LA U-Pb age
91 determination. Finally, the quantity of the WC1 sample that is currently available for future
92 work is limited and is likely to not fully meet the growing demands of the LA scientific
93 community; although, we note here that there is a potential for further sample collection from
94 the original site.

95 This contribution introduces a new carbonate reference material that can be widely used for *in-*
96 *situ* dating of calcite as primary or as cross-reference material with other available standards.
97 We characterise the reference material at various resolutions using a combination of (1) laser
98 ablation imaging (20 μm square beam); (2) LA spot analysis, $\sim 80\text{-}110$ μm in diameter,
99 conducted on both multi-collector (MC) and single collector inductively coupled plasma mass

100 spectrometer (ICPMS); and (3) ID-TIMS analyses of ~~36-37~~ sub-samples (~1-7 mg aliquots).
101 We discuss several key issues related to the use of ASH-15 sample as a RM, including down-
102 hole fractionation, heterogeneities, and previous bulk analyses, ~~and the possible effect of~~
103 ~~samples size and blank corrections~~, to provide the best correction parameters and suggested
104 protocols for users of the LA scientific community.

105

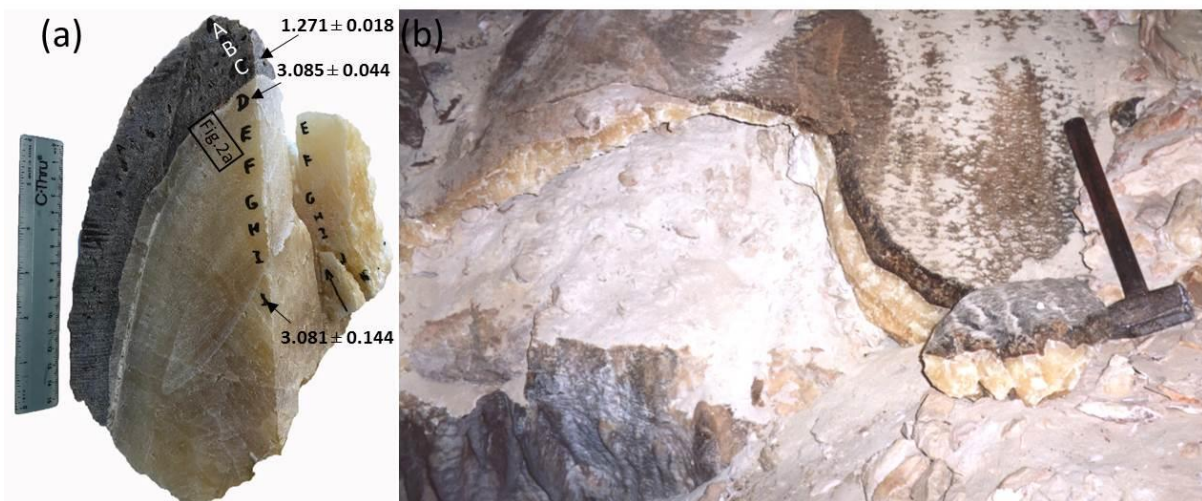
106 **1. The ASH-15 flowstone**

107 The ASH-15 flowstone was found in Ashalim Cave, a karstic cave in the central Negev Desert
108 (30°56'36.2" N, 34°44'22.5" E), southern Israel, which is part of the northern margin of the
109 Saharan–Arabian desert belt. The cave entrance is located at an elevation of 414 m above sea
110 level and 67 km SE from the Mediterranean Sea coast. The cave is a three-dimensional
111 hypogene maze with a total length of 540 m, situated in Turonian limestone rock strata, at
112 depths of 0-31 m below the surface. The cave is richly decorated with vadose speleothems,
113 such as stalagmites, stalactites and flowstone, which are not active today because of the aridity
114 of the climate in the area (Vaks et al, 2010, 2018), but periods of their deposition correspond
115 to past episodes of wet climate in present-day desert. The thickness of the speleothems varies
116 from several cm to a few tens of cm. The soil above the cave is silicate loess, originated mainly
117 from aeolian dust (Crouvi et al., 2010) and the present day vegetation is composed of sparse
118 xeric shrubs with <10% vegetation cover.

119 The vadose speleothems of Ashalim Cave are composed of low-Mg calcite, and are divided
120 into a relatively thick Pliocene Basal layer, and thinner Pleistocene layers above it. The Basal
121 layer varies from 5 to 25 cm in thickness and comprises c. 90% of the speleothem volume in
122 the cave. It is composed of massive yellow calcite crystals (Fig. 1a-b), often showing
123 continuous growth in stalagmites and flowstone, suggesting deposition from continuously

124 dripping water. In all speleothems the Basal layer is terminated at its top by a <1 mm layer of
125 microcrystalline calcite, evaporite minerals and reddish clays (Fig. 1a), that is interpreted as a
126 hiatus (growth break) separating the Basal Pliocene layer and Quaternary layers above it (Vaks
127 et al., 2013). The thickness of Pleistocene top layers varies from several mm to 17 cm, but
128 usually does not exceed a few cm, comprising about 10% of the speleothem volume in the cave.
129 It is composed of alternating layers of brown calcite, with the youngest top layer (where found)
130 composed of yellow calcite. Several variably colored layers <1 mm thick of microcrystalline
131 calcite, evaporite minerals and reddish clays are found within the columnar crystalline structure,
132 suggesting hiatuses in speleothem deposition (Vaks et al., 2013).

133 The youngest periods of speleothem deposition in several Ashalim Cave speleothems were
134 dated by the ^{238}U - ^{230}Th method and occurred from 221 ka to 190 ka and from 134 to 114 ka
135 (Vaks et al, 2010). Earlier periods of deposition were dated by the U-Pb method on ASH-15
136 flowstone ~~and are dated to~~ at 1.272 ± 0.018 Ma (ASH-15-C), and the Basal layer of ASH-15
137 flowstone (layers D-K) ~~dated to~~ at c. ~ 3.1 Ma (Fig 1a). These layers have been dated in three
138 different labs following several protocols for ID analysis (Vaks et al., 2013; Mason et al., 2013).
139 The U concentrations in speleothem calcite range between 1.9 and 19.7 $\mu\text{g/g}$ and the amounts
140 of non-radiogenic Th are negligible (Vaks et al., 2010).



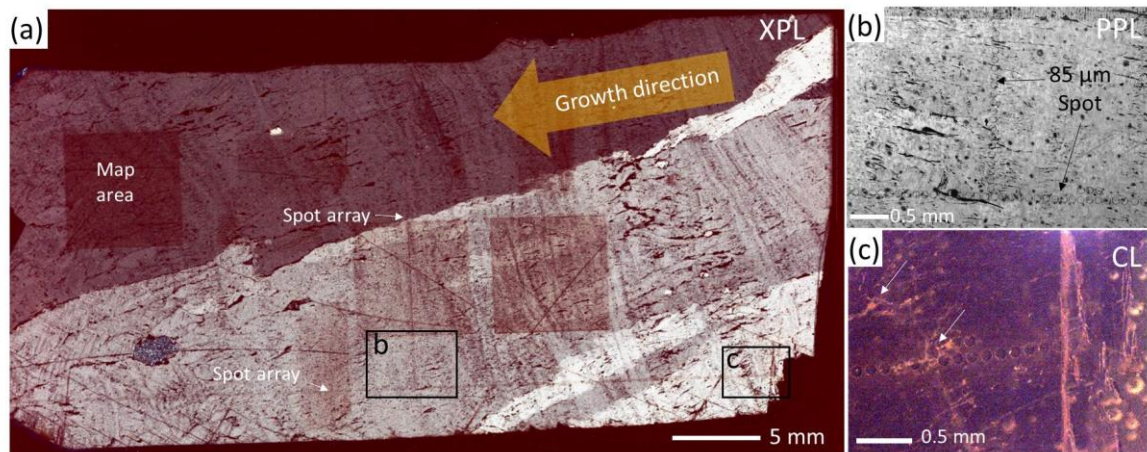
142 **Figure 1.** Sample ASH-15 from Ashalim Cave. (a) ~5 kg block of sample ASH-15 flowstone
143 consisting of the massive Pliocene yellow Basal layer (>2 cm calcite crystals; section D–K)
144 and the brown Quaternary layer (top section, A–C), the thin layer between the two stratigraphic
145 members represents a growth break (hiatus). The main U-Pb ages of Vaks et al., 2013 are
146 indicated; ~~-(b)~~ In-situ flowstone within Ashalim Cave from which ASH-15 was sampled,
147 showing the large reservoir of this flowstone.

148

149 2. Sample ASH-15 textural characterization

150 The ASH-15 thin-section includes section D and E ~~of the ASH-15 sample~~ (see location in
151 Fig.1a). Overall the thin-section examination indicates that the original texture is preserved
152 with consistent growth direction, no observed hiatus, and no indications for dissolution and
153 recrystallization. A spot analysis array, 85 µm in diameter, targeted along growth ~~bands-zone~~
154 and ~~perpendicular to along~~ -growth ~~direction are-is~~ visible in Fig. 2a-c. The ASH-15 sample
155 shows no luminescence under cathodoluminescence light (Fig. 2c), suggesting formation under
156 oxidising conditions. The slight bright luminescence observed within grain boundaries,
157 discontinuities, and veins (arrows in Fig. 2b-c) may suggest ~~for~~ the presence of fluid inclusions,
158 textural differences, or some local replacement within these areas. These areas should be
159 avoided if possible during spot analysis. The relatively homogenous low luminescence may
160 suggest for a single-phase continuous calcite growth, whereby precipitation occurred relatively
161 rapid from the same fluid source (e.g. with consistent Mn²⁺ Fe²⁺ composition) and/or under
162 similar precipitation redox conditions. This 15 cm thick, ~3 Ma Pliocene layer (section D-K)
163 is essentially of the same age. For this reason, previous dating of this sample also considered a
164 similar initial ²³⁴U/²³⁸U activity ratio for disequilibrium correction (Mason et al., 2013; Vaks
165 et al., 2013). The ASH-15 reference material consists of the whole Pliocene section that

166 terminates with a sharp transition to the darker Pleistocene layers above it (section A-C; see
 167 Fig. 1b). About 3 kg of ASH-15 sample are excavated from the Ashalim Cave (Fig. 1a), and
 168 potentially much more can be sampled in the future (we estimate more than 10 kg of sample;
 169 Fig. 1b). The ASH-15 flowstone is therefore a good candidate for a reference material because
 170 of its large volume, high U concentrations, and potentially homogenous age which will be
 171 examine next.



172
 173 **Figure 2.** ASH-15D-E thin-section. (a) cross-polarized (XPL) scan of ASH-15D-E thin-section,
 174 36 mm long, showing continuous growth (no hiatus), and consistent growth direction (indicated
 175 with yellow arrow). Spot analyses are targeted either sub-parallel to growth band-zone or
 176 perpendicular-sub-parallel to growth direction; (b) close-up on spot array analyses (location is
 177 shown in a) with 85 μm diameter; (c) CL image of the same area showing no luminescence
 178 and except for some bright luminescence within grains boundaries and veins (arrows).

179 3. Methods

180 3.1. Elemental mapping

181 The sample ASH-15 was cut perpendicular to the growth bands-zone of section D and E (see
 182 Fig. 1b) in order to examine heterogeneities across growth bands-zone and within. Thin-sections
 183 were then examined under plane- and cross-polarized light (XPL/PPL), and

184 cathodoluminescence (CL) microscopy (Fig. 2). The central part of the thin-section was also
185 analyzed for elemental distribution of selected elements. The elemental maps were measured
186 via LA-ICPMS, carried out on a 193 nm ArF excimer laser ablation system (Analyte G2
187 Teledyne Photon Machines Inc., Bozeman MT) coupled to an ICP-QMS (Agilent 7900, Agilent
188 Technologies, Santa Clara CA). The laser was equipped with a Photon Machines HelEx II
189 ablation chamber and an Aerosol Rapid Introduction System (ARIS). The experiments were
190 carried out using acquisition parameters (both on the ICP and on the laser) modelled using the
191 approach of van Elteren et al (2019; 2018) to avoid artefacts (e.g., aliasing, smear, blur). All
192 images (500x500 pixels) were acquired using a 20 μm square beam, fluence of 3.5 Jcm^{-2} , 294
193 Hz repetition rate and dosage of 10 (10 overlapping pulses per spot size which amounting to a
194 scanning speed of 588 μms^{-1}). The masses monitored were ~~^{24}Mg , ^{55}Mn , ^{63}Cu , ^{85}Rb~~ ^{88}Sr , ^{137}Ba ,
195 ^{206}Pb , ^{208}Pb , ^{232}Th , and ^{238}U and the images were constructed using Photon Machines' HDIP
196 data reduction software (van Malderen, 2017).

197 3.2. LA-MC-ICPMS spot analyses

198 A thin section of ASH-15 was dated by U-Pb laser ablation multi-collector inductively coupled
199 plasma mass spectrometry (LA-MC-ICPMS) following the method described in Nuriel et al.
200 (2017). A Nu Plasma 3D was employed in conjunction with a Photon Machines Excite 193nm
201 Excimer laser equipped with a HelEx two volume cell. The laser was fired for 15 s during
202 analysis, using a ~~re~~repetition rate of 10 Hz, a spot size of 85 μm , and a fluence of approx. 1
203 J/cm^2 . The Nu Plasma 3D allows for the simultaneous acquisition of ^{238}U , ^{235}U , ^{232}Th , ^{208}Pb ,
204 ^{207}Pb , ^{206}Pb , ^{204}Pb (+Hg), and ^{202}Hg , where ^{238}U - ^{232}Th are measured on Faraday detectors and
205 the low-side masses are measured on Daly detectors. Instrumental mass-bias was corrected
206 using a two-step approach: both the $^{207}\text{Pb}/^{206}\text{Pb}$ and $^{206}\text{Pb}/^{238}\text{U}$ ratios were first corrected to
207 NIST-614 glass reference material in *Iolite 3* using the geochronology reduction scheme (Paton
208 et al., 2010) to account for both mass-bias ($^{207}\text{Pb}/^{206}\text{Pb}$) and instrumental drift ($^{207}\text{Pb}/^{206}\text{Pb}$ and

209 $^{206}\text{Pb}/^{238}\text{U}$). The Tera-Wasserburg data, output from *Iolite*, was then plotted and $^{206}\text{Pb}/^{238}\text{U}$
210 ratios of all RMs and unknowns were adjusted such that the primary calcite reference
211 material—WC-1—yielded an age of 254 Ma (Roberts et al., 2017). This resulted in accurate
212 dates for both our secondary calcite RMs; Duff Brown Tank at -66.8 ± 3.4 Ma (previously
213 reported 64 Ma; Hill et al., 2016) and a $^{207}\text{Pb}/^{206}\text{Pb}$ date of zircon RM at 566.0 ± 2.8 Ma
214 (previously reported Sri Lanka, 564 Ma; Gehrels et al., 2008), of 66.8 ± 3.4 Ma and a $^{207}\text{Pb}/^{206}\text{Pb}$
215 date of a 566.0 ± 2.8 Ma. Uncertainty propagation of individual ratios was assessed by
216 reproducibility of the NIST614 and SL RMs (n=44 in both cases) and added in quadrature such
217 that the MSWD of each weighted average is ≤ 1 and that the uncertainty is no better than 2%
218 (long-term reproducibility); this resulted in propagated uncertainties of 2.5% and 2% for the
219 $^{206}\text{Pb}/^{238}\text{U}$ and $^{207}\text{Pb}/^{206}\text{Pb}$ ratios, respectively. Given that the typical uncertainties of the
220 $^{206}\text{Pb}/^{238}\text{U}$ and $^{207}\text{Pb}/^{206}\text{Pb}$ ratios of the unknowns was $>10\%$ and $>3\%$, respectively, the
221 uncertainty propagation on individual ratios had little effect on the calculation of the final date
222 of ASH-15. The thin section of ASH-15 was measured both parallel to the length of section
223 (303 spots, and perpendicular to it (101 spots). Data are plotted using Isoplot (Ludwig, 1998).

224 3.3. LA-ICPMS spot analyses

225 Analyses were conducted at the Geochronology and Tracers Facility, British Geological
226 Survey (Nottingham, UK). The instrumentation comprised a New Wave Research 193UC
227 excimer laser ablation system fitted with a TV2 cell, coupled to a Nu Instruments Attom single
228 collector inductively coupled plasma mass spectrometer (ICP-MS). The method follows the
229 protocols described in Roberts and Walker (2016) and Roberts et al. (2017). Laser parameters
230 varied slightly per session, but typically involve a pre-ablation cleaning spot of $150\ \mu\text{m}$, fired
231 at 10 Hz with a fluence of $\sim 6\ \text{J}/\text{cm}^2$ for 2 seconds, and ablation conditions of 80-100 μm spots,
232 fired at 10 Hz with a fluence of $\sim 6-8\ \text{J}/\text{cm}^2$ for 25-30 seconds. A 60 second background is taken
233 before every set of standard-bracketed analyses, and a 5 second washout is left between each

234 ablation. Normalization of Pb-Pb ratios is achieved using NIST614 glass (values of Woodhead
235 and Hergt, 2001), and WC-1 carbonate for Pb-U ratios (Roberts et al., 2017). Data reduction
236 uses the Time Resolved Analysis function of the Nu Instruments Attolab software, and an excel
237 spreadsheet, with uncertainty propagation following the recommendations of Horstwood et al.
238 (2016).

239

240 **3.4. ID-TIMS U-Pb geochronology**

241 Isotope dilution thermal ionization mass spectrometry (ID-TIMS) U-Pb geochronology was
242 performed at the Institute of Geochemistry and Petrology of ETH Zurich (ETHZ) and at the
243 Department of Earth Sciences of the University of Geneva (UNIGE). Millimeter-sized chips
244 of the ASH-15-D and ASH-15-K calcite were extracted using stainless steel tools. Larger chips
245 were further sub-divided resulting in ~1-7 mg aliquots. Individual chips were transferred into
246 3 ml Savillex beakers and repeatedly ultrasonically cleaned in ultrapure acetone and water.
247 Cleaned samples were transferred into pre-cleaned 3 ml Savillex beakers, spiked with ~5-10
248 mg EARTHTIME (^{202}Pb - ^{205}Pb - ^{233}U - ^{235}U) tracer solution (Condon et al., 2015) and dissolved
249 in 6N HCl at 120°C on a hotplate for ~30 minutes to assure complete dissolution and sample-
250 spike equilibration. Dissolved samples were dried down and redissolved in 1N HBr. Uranium
251 and Pb were separated using a single-column (50 μl , AG1-X8 resin) HBr-HCl anion exchange
252 chemistry. The Pb fraction was dried down with a drop of H_3PO_4 after a single column pass.
253 Uranium was dried down, redissolved in 3N HCl and further purified with a HCl-based second
254 column pass before drying it down with a drop of H_3PO_4 . Uranium and Pb were loaded on
255 outgassed single Re filaments with ~1 μl of Si-gel emitter for thermal ionization mass
256 spectrometry. Uranium and Pb isotope ratios were measured on a Thermo TRITON Plus at
257 ETHZ and a Thermo TRITON at UNIGE. Lead isotopes were measured on the axial secondary

258 electron multiplier employing dynamic peak-hopping routine collecting masses (202), 204, 205,
259 206, 207 and 208. Measured Pb isotope ratios were corrected for mass fractionation either using
260 the double spike (ETHZ) or using a mass fractionation factor of 0.15 ± 0.03 ‰/amu for single
261 Pb spiked samples (UNIGE). Uranium isotope ratios were measured as uranium-oxide (UO₂)
262 employing a static measurement routine with Faraday cups connected to amplifiers with 10^{13}
263 ohm feedback resistors (von Quadt et al., 2016; Wotzlaw et al., 2017). Isotope ratios were
264 corrected for isobaric interferences from minor UO₂ isotopologues (Wotzlaw et al., 2017) and
265 for mass fractionation using the double spike assuming a $^{238}\text{U}/^{235}\text{U}$ ratio of 137.818 ± 0.045
266 (Hiess et al., 2012) for sample and blank. Total procedural Pb blanks for the HBr-based
267 chemistry at ETHZ are consistently between 0.2 and 0.4 pg. We therefore attribute up to 0.4
268 pg to laboratory blank with the remaining common Pb being attributed to initial common Pb.
269 Total procedural blanks measured at UNIGE yielded an average of 1.15 pg that was taken as
270 the laboratory blank contribution. Data reduction and uncertainty propagation was performed
271 using Tripoli and an Microsoft Excel-based spreadsheet that uses the algorithms of Schmitz
272 and Schoene (2007). Isochron calculations were performed using IsoplotR (Vermeesch, 2018).
273 All uncertainties are reported at 95% confidence ignoring systematic uncertainties associated
274 with the tracer calibration and decay constants unless otherwise stated.

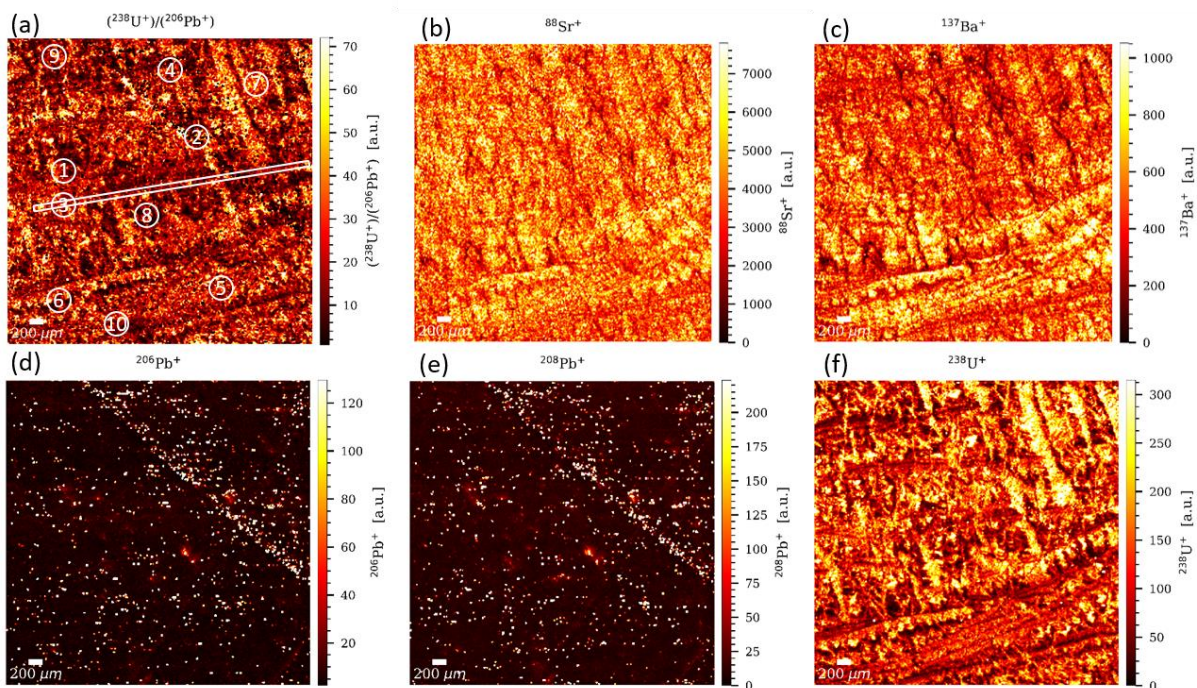
275 **4. Results**

276 All analyses were performed on ASH-15-D-K yellow Pliocene layer, abbreviated here as
277 “ASH-15” unless specification of ASH-15-D, E etc. is indicated. The ASH-15-A-C brown
278 Pleistocene layer is not part of the ASH-15 suggested reference material.

279 **4.1. LA elemental mapping**

280 Elemental mapping for ^{88}Sr , ^{137}Ba , ^{206}Pb , ^{208}Pb , ^{238}U and $^{238}\text{U}/^{206}\text{Pb}$ ratio shows that the
281 distribution of most elements is relatively homogeneous (Fig.3), and in good accordance with

282 the luminescence data. Higher intensities for ^{238}U and ^{88}Sr were observed along grain
 283 boundaries and discontinuities, whereas Pb and the rest of the trace elements are more
 284 homogeneously distributed, arguing for steady environmental conditions ~~that have kept steady~~
 285 during the deposition. Ten random regions of interest (ROI) were selected throughout the
 286 sample to mimic 10 spot analysis carried out at 85-90 microns spot size – just like one would
 287 do for U-Pb geochronology, ~~for example~~. These ROIs were generated by drawing on the map
 288 circular regions with the radius of 85 or 90 microns in diameter. The pixels comprising each
 289 ROI were pooled together as representing the equivalent of a single spot analysis. The statistical
 290 data for each cluster (data are given in supplementary file) ~~was-were~~ compared. The average
 291 values for all pixel data ~~is-are~~ within 2 standard errors and in good agreement, indicating that,
 292 at least based on the elemental distribution we measured, the sample is relatively homogeneous
 293 for a natural sample. To further investigate the chemical homogeneity of the sample, a random
 294 transect through one of the growth zones was drawn and the signal intensities for ^{238}U were
 295 extracted. The transect data also indicate that ^{238}U variations are within 2 standard errors of the
 296 average value- (full data is available in Table S1 in the supplement).



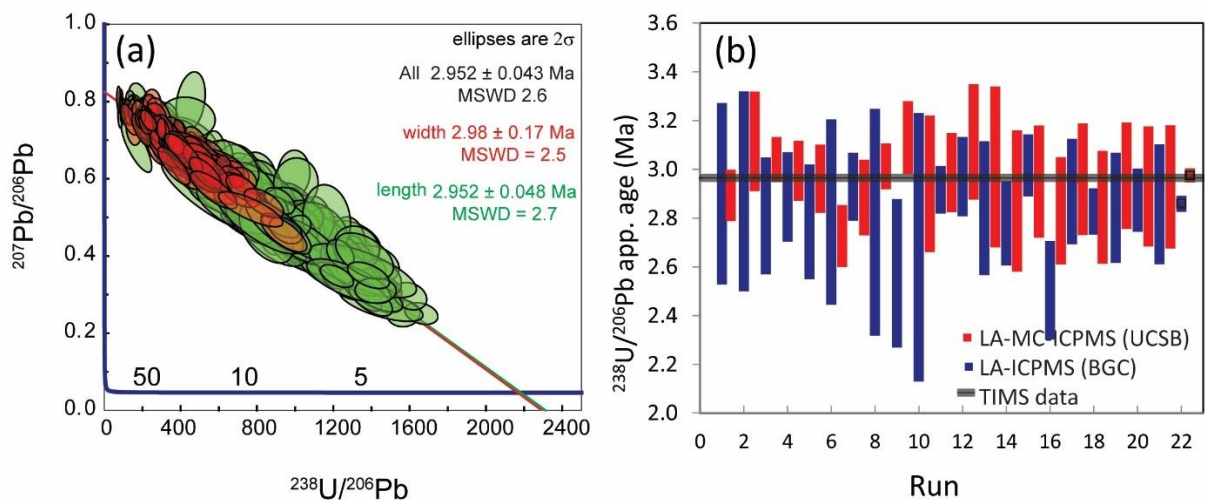
298 **Figure 3.** Signal intensity maps of ASH-15. for $^{238}\text{U}/^{206}\text{Pb}$, ^{88}Sr , ^{137}Ba , ^{206}Pb , ^{208}Pb , and ^{238}U
299 (a-d). The plotted signal was corrected for blank and analytical drift of the instrumentation.
300 Note that each distribution map has its own signal intensity scale. The position of the regions
301 of interest and transect is shown in (a). The circles designating the location of the regions of
302 interest are not at scale. (data is available in Table S1 in the supplement).

303 **4.2. LA-MC-ICPMS spot analyses**

304 Data and calculated ages for the LA-ICPMS transects are shown in Tera-Wasserburg space in
305 Fig. 4 (n = 379 of 412 total spots). Analyses rejected from the age calculation include those
306 with $^{207}\text{Pb}/^{206}\text{Pb}$ uncertainties larger than 0.1% (n = 2) and those with high common-Pb contents
307 (^{208}Pb cps >5000; n = 17). A further 14 spots plotted below the array; these data ~~were represent~~
308 the first 1–2 mm of spots of the lengthwise transect (lower right in Fig. 2a), and suggest that a
309 small percent of ASH-15 may behave differently during ablation and/or may have been
310 subsequently modified after crystallization; upon inspection, this portion of the section contains
311 more pore space and impurities than the majority of the section. The remaining 379 define a
312 normally distributed array with a lower intercept age of 2.952 ± 0.043 Ma (MSWD = 2.5),
313 which is well within uncertainty of the new ID-TIMS data presented ~~herein~~ (full data is available
314 in Table S2 in the supplement) ~~and the scatter observed in the LA data (i.e., MSWD > 1) is~~
315 ~~lower compared with scatter observed in the ID-TIMS data.~~ The calculated upper intercept of
316 each transect is equivalent and within 1% of the common Pb composition calculated from the
317 ID-TIMS data. Not surprisingly, the lengthwise transect reveals a larger spread in
318 common/radiogenic Pb ratios; this transect crosses more growth zones and has a higher
319 probability of sampling a variety of concentrations of both Pb and U. Conversely, the more
320 limited spread in common/radiogenic Pb ratios appears to reflect the limited sampling of
321 growth zones, and would suggest that individual growth zones contain a relatively limited
322 range of concentrations in U and Pb. The slightly higher MSWD for the lengthwise transect

323 (2.7) relative to the growth zone transect (2.5) could also reflect these inherited compositional
 324 differences during growth history, and a resulted “mixing” or “averaging” of different growth
 325 phase along calcite continuous growth.

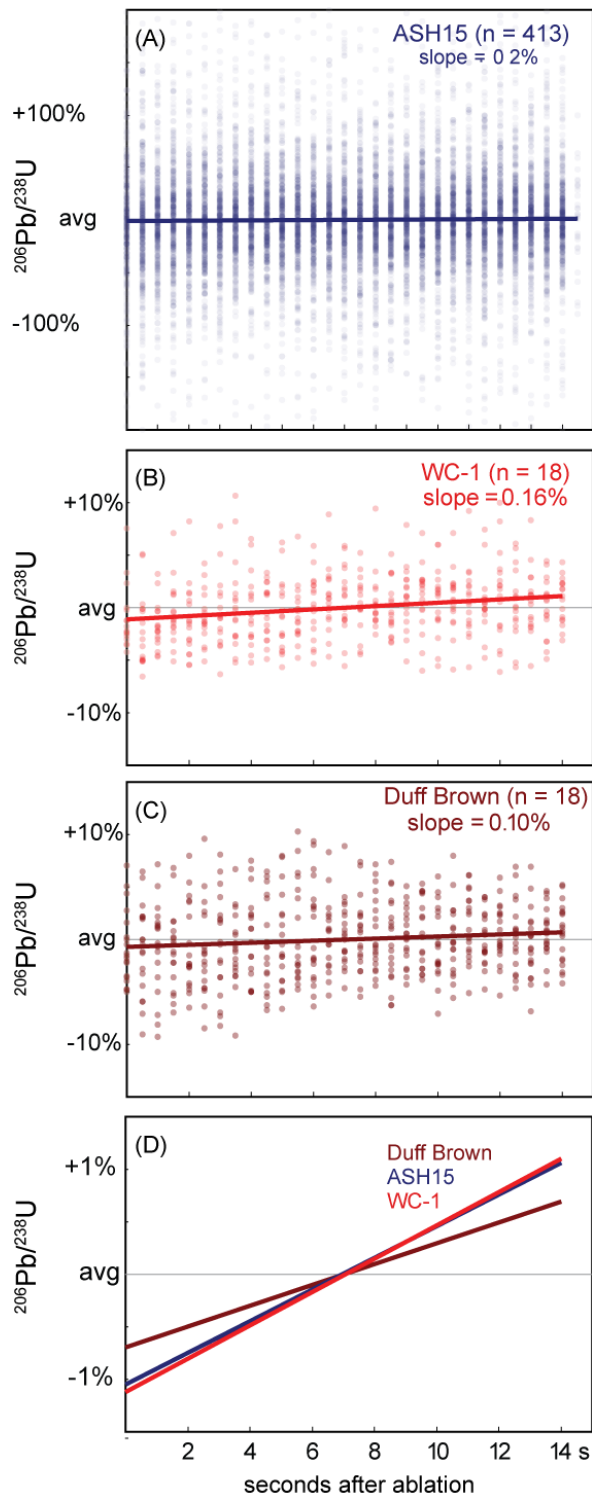
326 Variations of ASH-15 ages during 20 different runs (with 5-30 spot analysis in each) using
 327 both single (ICPMS) and multi-collector (MC-ICPM) are shown in Fig. 4b (full data is available
 328 in Tables S3-S5 in the supplement). The ages are calculated using IsoplotR, not anchored to
 329 0.8315-specific common-lead, and are not corrected for disequilibrium. Although there is a
 330 large scatter in the ages of the different runs the average ages (marked in with black box thick
 331 lines) are plotted close to the new ID-TIMS ages, or are slightly younger in age.



332
 333 **Figure 4.** LA-MC-ICPMS analyses of calcite ASH-15. (a) Tera-Wasserburg concordia space
 334 plot (n=385) for (n=385). Spots-spots analysis within lengthwise transect (green) and along
 335 growth zone transect (red). Calculated age, 2σ error and MSWD are given for both and for all
 336 spots together; (full data is available in Table S2 in the supplement); (b) Variations of ASH-15
 337 ages during different runs using both single and multi-collector ICPMS. Ages are calculated
 338 using WC1 as primary MS; the new ID-TIMS age is indicated with a grey line; (full data is
 339 available in Table S3-S5 in the supplement) Ages are calculated using IsoplotR, anchored to
 340 0.8315 common-lead, and are not corrected for disequilibrium.

341 4.3. Down-hole fractionation

342 Reference material is important for correction of both laser-induced elemental fractionation
343 (LIEF) and ~~in~~-plasma-related ionization efficiency. Ideally, the reference material should
344 resemble the unknown samples as much as possible in terms of its chemistry (e.g. Mg and Fe
345 content), texture (i.e. micritic, crystalline), and age. The WC1 and ASH15 are both low-Mg
346 calcite but they are very different in ~~their~~-textures and age. The ASH15 is a ~3 Ma, well-
347 crystallized elongated calcite (up to 1 cm) and WC1 is a 254 Ma recrystallized botryoidal
348 calcite, formed after aragonite. Despite these differences, both WC1 and ASH15 display a very
349 similar down-hole fractionation pattern (Fig. 5d). Fig. 5 shows stacked integration plots of the
350 down-hole raw $^{206}\text{Pb}/^{238}\text{U}$ ratio of different RMs including, the ASH15, WC-1, and Duff
351 Brown Tank (Black and Gulson, 1978). The ASH15 displays s much larger scatter in the raw
352 data (Fig. 5a) in comparison to both WC1 and Duff Brown Tank (Fig. 5b-c), however, the
353 average value yielded identical down-hole ~~patterns-fractionation~~ to that of WC-1 (Fig. 5d).
354 Duff Brown Tank is also consistent with the down-hole patterns ~~but~~ less steep in comparison
355 to WC1 and ASH15 (Fig. 5d). This comparison suggests s that down-hole fractionation and
356 laser-induced elemental fractionation (LIEF) ~~is-are~~ similar among the different RMs. It is thus
357 suggested that differences in measured and expected $^{206}\text{Pb}/^{238}\text{U}$ ratios ~~between-measured-and~~
358 ~~expected~~-in calcite material are likely to be caused mostly by plasma-ionization differences
359 between unknown samples and RMs.



360

361 **Figure 5.** Stacked integration plots of raw ^{207}Pb -corrected $^{206}\text{Pb}/^{238}\text{U}$ ratios for calcite reference
 362 materials ASH-15, WC-1, and Duff Brown Tank. The low Pb concentration in ASH-15 yields
 363 more scatter, but average slopes of all RMs are similar, with 1-2% change in age over 10
 364 seconds (100 pulses) of ablation. The results suggest ~~for~~ minimal differences in down-hole
 365 fractionation of the different RMs.

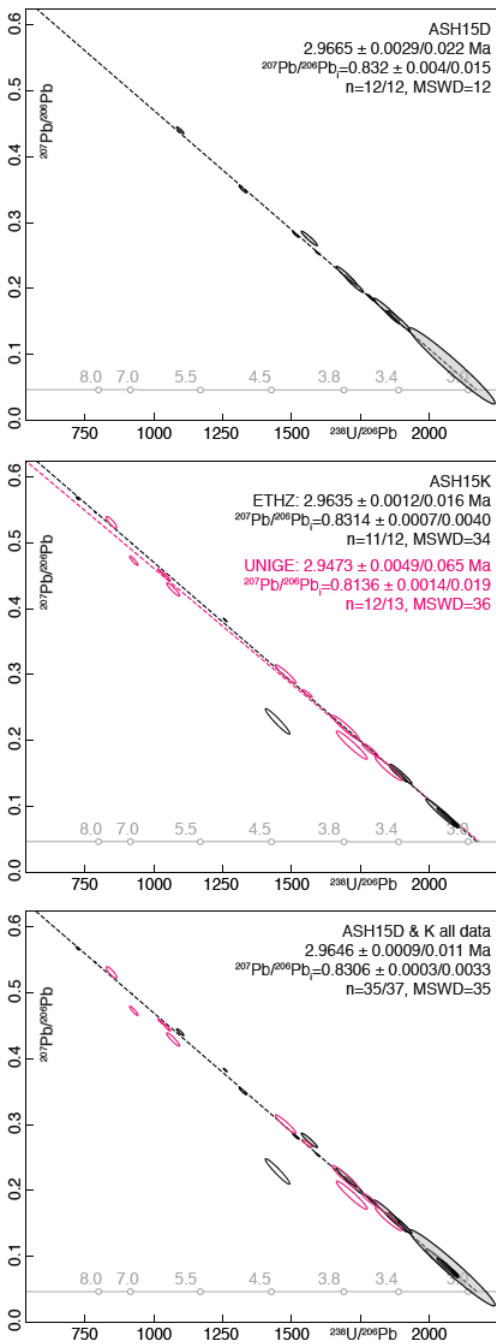
366 4.4. ID-TIMS results

367 Twelve aliquots of ASH-15D analyzed at ETHZ yielded $^{238}\text{U}/^{206}\text{Pb}$ ratios between 1096 and
368 2084 and $^{207}\text{Pb}/^{206}\text{Pb}$ ratios between 0.0825 and 0.4403 ([full data is available in Table S6 in the](#)
369 [supplement](#)). Plotted in Tera-Wasserburg space, ~~this~~ these data yields a single isochron with an
370 initial $^{207}\text{Pb}/^{206}\text{Pb}$ of 0.832 ± 0.015 (uncertainties are 95% confidence intervals) and a concordia
371 intercept age of 2.967 ± 0.022 Ma (Fig. 6a). The elevated mean square weighted deviation
372 (MSWD) of 12 is attributed to minor heterogeneities, most likely in the initial $^{207}\text{Pb}/^{206}\text{Pb}$ ratio
373 of the speleothem calcite. Twelve aliquots of ASH-15K analysed at ETHZ returned $^{238}\text{U}/^{206}\text{Pb}$
374 ratios between 723 and 2094 and $^{207}\text{Pb}/^{206}\text{Pb}$ ratios between 0.0720 and 0.5677. In Tera-
375 Wasserburg space, eleven out of twelve aliquots define a isochron with an initial $^{207}\text{Pb}/^{206}\text{Pb}$ of
376 0.8314 ± 0.0040 and a concordia intercept age of 2.964 ± 0.016 Ma (Fig. 6b). A single aliquot
377 (#5.4) plots significantly below the isochron defined by the other aliquots. The elevated MSWD
378 of 34 together with the single outlier suggest some heterogeneities in the initial $^{207}\text{Pb}/^{206}\text{Pb}$ of
379 the ASH-15K calcite. Thirteen aliquots of ASH-15K analysed at UNIGE (pink color, Fig. 6b)
380 yielded $^{238}\text{U}/^{206}\text{Pb}$ ratios between 433 and 1853 and $^{207}\text{Pb}/^{206}\text{Pb}$ ratios ranging from 0.1856
381 to 0.6660. Twelve of the thirteen analyses yield ~~define an~~ best-fit isochron ~~isochron-line~~ with an
382 initial $^{207}\text{Pb}/^{206}\text{Pb}$ of 0.814 ± 0.019 and a Concordia intercept age of 2.947 ± 0.065 Ma. The
383 elevated MSWD of 36 confirms the minor heterogeneity of the initial $^{207}\text{Pb}/^{206}\text{Pb}$.

384 The excellent agreement between the ASH-15D and ASH-15K datasets ~~suggest~~ indicates that
385 the entire speleothem growth layer between these two growth zones is of equivalent age with
386 minor heterogeneities in the initial $^{207}\text{Pb}/^{206}\text{Pb}$ ratio and justifies combining the data into a
387 single isochron regression. The combined isochron, using 35 of 37 analysed aliquots, yields an
388 initial $^{207}\text{Pb}/^{206}\text{Pb}$ of 0.8306 ± 0.0033 and a concordia intercept age of 2.965 ± 0.011 Ma with
389 a MSWD of 35 (Fig. 6c). We consider the results of the combined ~~isochron~~ regression as the
390 best reference value for using ASH-15 as a primary reference material.

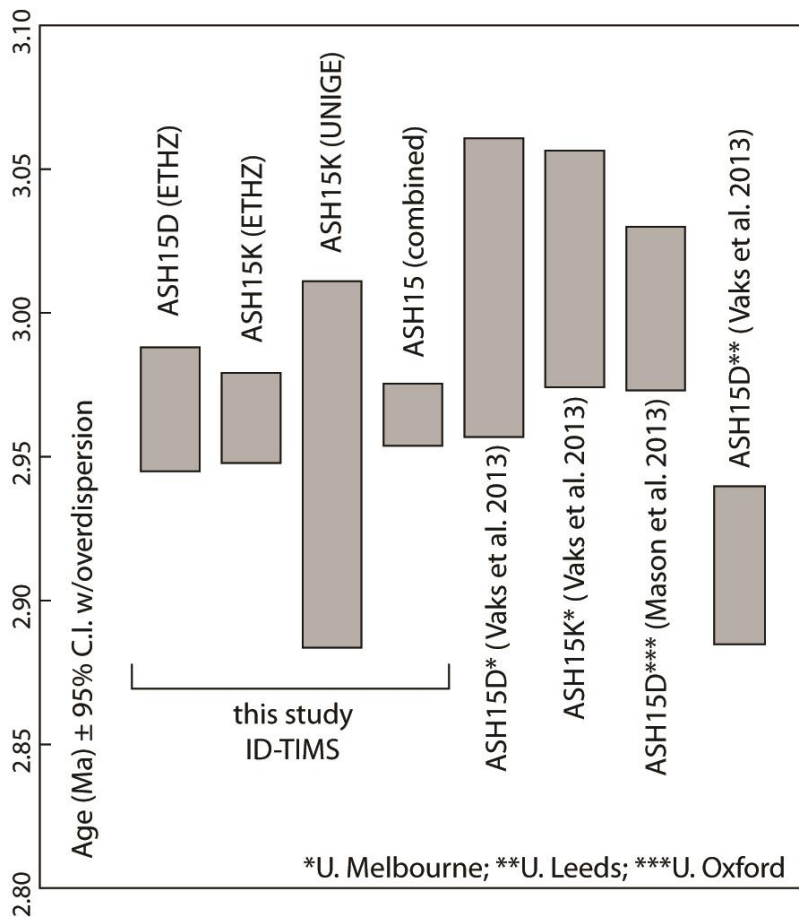
391 The new TIMS data provide the most extended bulk ~~investigation-analyses work~~ of the ASH-
392 15 sample, with a total of 37 sub-samples that are separated from bottom (K, n=25) to top (D,
393 n=12) ~~sections of the sample~~. The ~~relatively~~ high MSWD of 35 is suggested to reflect true
394 heterogeneities of the dated material, possibly related to impurities that are concentrated within
395 grain boundaries (as suggested by CL and elemental mapping). We re-calculated previously
396 determined isochron ages of Vaks et al. (2013) and Mason et al. (2013; Fig. 7). We obtained
397 concordia intercept ages of 3.0088 ± 0.053 Ma for ASH-15-D (MSWD=11; n=5) and 3.0153
398 ± 0.042 Ma for ASH-15-K (MSWD=14; n=5) of Vaks et al. (2013) and 3.0015 ± 0.029 for
399 ASH-15-D (MSWD=2; n=5) of Mason et al. (2013). These ages ~~are systematically older but~~
400 ~~still overlap within uncertainty with~~ are largely overlapping within uncertainty with our new
401 ID-TIMS age of 2.965 ± 0.011 Ma (Fig. 7; and data in Table S7 in the supplements). The
402 apparent minor systematic offset towards slightly older ages is attributed to the lower number
403 of aliquots in the MC-ICPMS datasets combined with the heterogeneous initial Pb isotope
404 composition. ~~We speculate that the small but systematic offset between previous results and~~
405 ~~our new data may be related to natural heterogeneities that are sampled differently depending~~
406 ~~on sample size but we cannot exclude analytical differences as an additional source of bias.~~
407 ~~The origin of this bias between the two techniques should be investigated more systematically~~
408 ~~in future~~. For laser ablation U-Pb work, we recommend the use of the new ID-TIMS age
409 because of the large number of sub-samples (n=37), and the small aliquots (1-7 mg) that are
410 more representative of laser-ablation spot analysis. In addition, the use of the precisely and
411 accurately calibrated EARTHTIME tracer solutions (Condon et al., 2015) and the online mass
412 fractionation correction provided by the double Pb and double U tracer are an important
413 advantage of this method ~~compared to previous bulk analyses~~. The excellent interlaboratory
414 reproducibility gives us additional confidences that our ID-TIMS data provide the most

415 accurate characterization of the U-Pb systematics of the ASH-15 calcite for use as a primary
416 reference material.



417

418 **Figure 6.** ID-TIMS U-Pb results for ASH-15D, ASH-15K, and for both ASH-15D+K
419 displayed in Tera-Wasserburg concordia space. Uncertainties on the initial $^{207}\text{Pb}/^{206}\text{Pb}$ ratios
420 and the intercept ages are given as 2σ and as 95% confidence intervals including overdispersion
421 (Vermeesch, 2018).



422

423 **Figure 7.** Previous (re-calculated) and new ages of ASH-15 from isotope-dilution U-Pb
 424 analysis. All ages are calculated using IsoplotR (Vermeesch, 2018), and are not corrected for
 425 disequilibrium and are not anchored to common-lead specific value (see data in Table S7 in
 426 the supplements).

427 **4.5. Calcite reference material**

428 The U and Pb concentrations of carbonate materials vary greatly. Data compilation by Roberts
 429 et al. (2020; this issue) combined hundreds of carbonate samples from different origin such as
 430 diagenetic, biogenic, speleothem, and vein-fill. This compilation indicates several orders of
 431 magnitude differences in U and Pb concentrations of the different types of carbonate and the
 432 heterogeneity of spot analysis within each type or even a single sample. A modified
 433 representation of their data, excluding calcite vein-fill, which vary throughout the entire

434 compositional range, is shown together with the currently available calcite reference materials
435 (Fig. 8; and full data in Table S8 in the supplement). Note that both ASH15 and JT, display
436 much larger heterogeneity when measured by LA-ICPMS (small symbols) relative to ID-TIMS
437 (large symbols). Despite the high compositional heterogeneity of each of the reference material,
438 they show minimal overlap and together they cover most of the compositional range of the
439 presented carbonate material. WC1 (Roberts et al., 2017) with relatively high U and Pb
440 concentrations can easily be measured on single collector ICPMS (including quadrupole
441 instruments) and is most appropriate to be used for dating vein-fill and diagenetic carbonates.
442 In contrast, the ASH15 flowstone, with relatively low Pb and high U concentration that are
443 better measured on sector-field (MC)-ICPMS is most appropriate for dating speleothem type
444 carbonates. Finally the JT (Guillong et al., 2020), with moderate U and Pb concentration can
445 be used on both single- and multi-collector sector field ICPMS instruments and for all types of
446 carbonate samples. Reference material with high Pb and low U or both low U and Pb
447 concentrations will further help to cover the full compositional range of carbonate material but
448 may introduce analytical challenges.

449

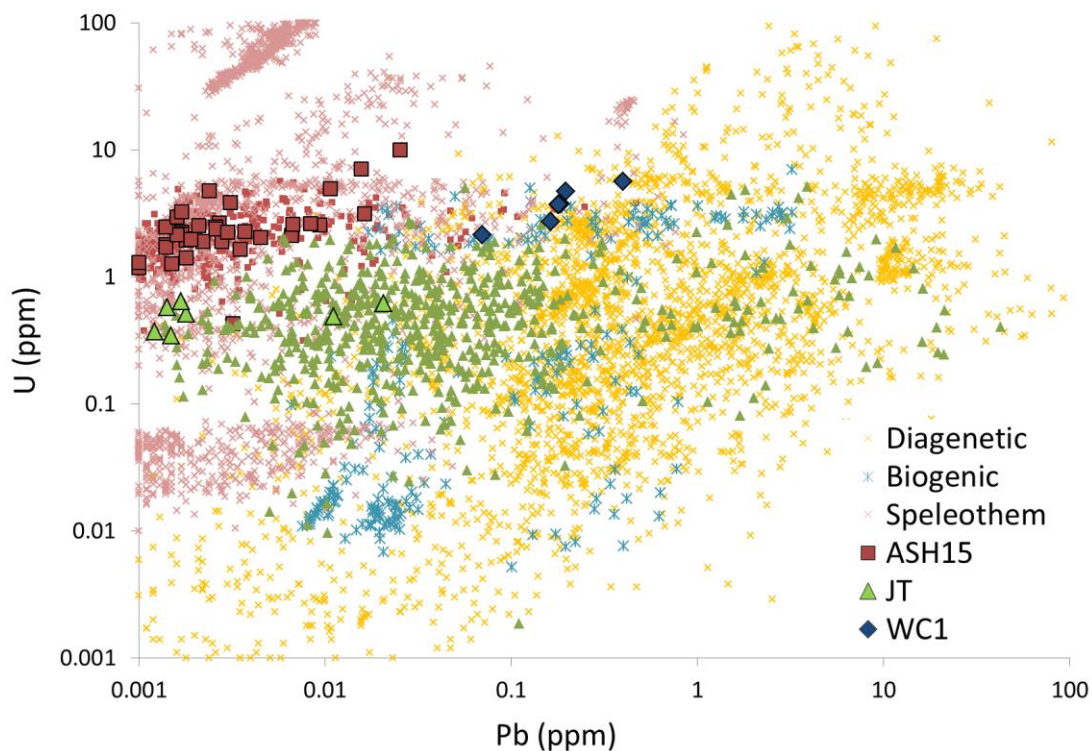


Figure 8. U and Pb concentrations of different carbonate samples and available reference materials. Large and small symbols for the reference materials indicate ID-TIMS and LA-ICPMS analyses, respectively. Note the minimal compositional overlap of the three reference materials (ASH15, WC1, and JT). Data for diagenetic, biogenic, and speleothem carbonates are from Roberts et al. (2020, this issue). Data for JT standard are from Guillong et al. (2020).

5. Conclusions

The ASH-15 speleothem calcite is characterized as a matrix matched reference material for LA-ICPMS U-Pb geochronology of calcite. ID-TIMS analyses of small 1-7 mg aliquots of two growth zones suggest sufficient homogeneity with a combined intercept age of 2.965 ± 0.011 Ma and an initial $^{207}\text{Pb}/^{206}\text{Pb}$ of 0.8315 ± 0.0026 . These data are recommended as the reference values for the ASH-15 calcite reference material. The excellent agreement between the two growth zones suggest that the entire interval between the two dated layers can be used with the same reference age. Compared to other calcite reference material (e.g. WC1), ASH-15 is more

465 homogeneous but has lower radiogenic Pb content and therefore requires more sensitive
466 instruments (i.e. sector field rather than quadrupole mass spectrometers) to be used as a
467 reference material.

468

469 **Author's contribution**

470 PN: data processing and writing, JFW: ID-TIMS analysis and writing, MO: ID-TIMS
471 analysis, AV: sample collection and writing, CS: LA mapping analysis and writing, MS: LA
472 mapping analysis. NR: LA-ICPMS, data analysis and writing. AKC: LA-MC-ICPMS, data
473 analysis and writing.

474

475 **Competing interests**

476 The authors declare that they have no conflict of interest.

477

478 **Acknowledgements**

479 We thank reviewers Fernando Corfu and Jon Woodhead as well as editor Axel Gerdes for
480 constructive comments and suggestions. We thank Bar Elisha for thin-section preparation and
481 ~~to~~ Andrew Mason for constructive discussion. This study was funded by the Israel Science
482 Foundation, Grant ISF-727/16.

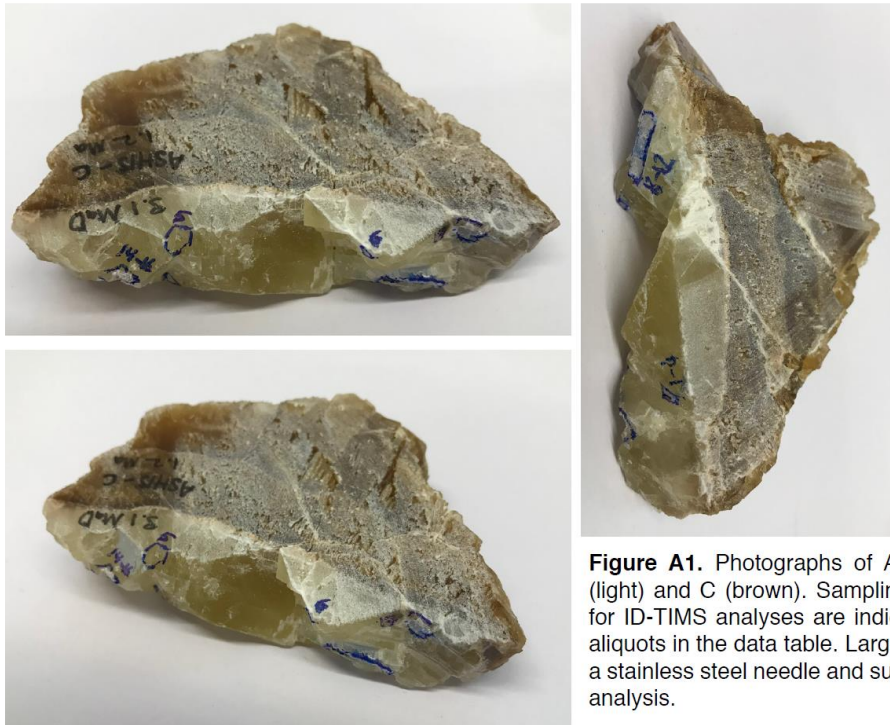


Figure A1. Photographs of ASH15 flowstone with layers D (light) and C (brown). Sampling localities of aliquots sampled for ID-TIMS analyses are indicated by numbers matching the aliquots in the data table. Larger pieces were chipped off using a stainless steel needle and subdivided into smaller aliquots for analysis.

484



Figure A2. Photographs of ASH15 flowstone with layers K (bottom) to D (top). Sampling localities of aliquots samples for ID-TIMS analyses within layer K are indicated with numbers (n=12) and are matching the aliquots in the data table.

485

486 **References:**

- 487 Anjiang, S., Anping, H., Cheng, T., Liang, F., Wenqing, P., Yuexing, F., and Zhao, J.: Laser ablation
488 in situ U-Pb dating and its application to diagenesis-porosity evolution of carbonate reservoirs, 46,
489 1127-1140, 2019.
- 490 Condon, D., Schoene, B., McLean, N., Bowring, S., and Parrish, R.: Metrology and traceability of U–
491 Pb isotope dilution geochronology (EARTHTIME Tracer Calibration Part I), *Geochimica et*
492 *Cosmochimica Acta*, 164, 464-480, 2015.
- 493 Coogan, L. A., Parrish, R. R., and Roberts, N. M.: Early hydrothermal carbon uptake by the upper
494 oceanic crust: Insight from in situ U-Pb dating, *Geology*, 44, 147-150, 2016.
- 495 Crouvi, O., Amit, R., Enzel, Y., and Gillespie, A. R.: Active sand seas and the formation of desert loess,
496 *Quaternary Science Reviews*, 29, 2087-2098, 2010.
- 497 Godeau, N., Deschamps, P., Guihou, A., Leonide, P., Tendil, A., Gerdes, A., Hamelin, B., and Girard,
498 J.-P. J. G.: U-Pb dating of calcite cement and diagenetic history in microporous carbonate reservoirs:
499 Case of the Urgonian Limestone, France, 46, 247-250, 2018.
- 500 Goodfellow, B. W., Viola, G., Bingen, B., Nuriel, P., and Kylander-Clark, A. R. C.: Palaeocene faulting
501 in SE Sweden from U–Pb dating of slickenfibres calcite, *Terra Nova*, n/a-n/a, 10.1111/ter.12280, 2017.
- 502 Guillong, M., Wotzlaw, J. F., Looser, N., and Laurent, O.: New analytical and data evaluation protocols
503 to improve the reliability of U-Pb LA-ICP-MS carbonate dating, *Geochronology Discuss.*, 2020, 1-17,
504 10.5194/gchron-2019-20, 2020.
- 505 Hansman, R. J., Albert, R., Gerdes, A., and Ring, U.: Absolute ages of multiple generations of brittle
506 structures by U-Pb dating of calcite, *Geology*, 46, 207-210, 2018.
- 507 Hiess, J., Condon, D. J., McLean, N., and Noble, S. R.: $^{238}\text{U}/^{235}\text{U}$ systematics in terrestrial uranium-
508 bearing minerals, *Science*, 335, 1610-1614, 2012.
- 509 Holdsworth, R., McCaffrey, K., Dempsey, E., Roberts, N., Hardman, K., Morton, A., Feely, M., Hunt,
510 J., Conway, A., and Robertson, A.: Natural fracture propping and earthquake-induced oil migration in
511 fractured basement reservoirs, *Geology*, 47, 700-704, 2019.
- 512 Horstwood, M. S., Košler, J., Gehrels, G., Jackson, S. E., McLean, N. M., Paton, C., Pearson, N. J.,
513 Sircombe, K., Sylvester, P., and Vermeesch, P.: Community-derived standards for LA-ICP-MS U-(Th-)
514 Pb geochronology—Uncertainty propagation, age interpretation and data reporting, *Geostandards and*
515 *Geoanalytical Research*, 40, 311-332, 2016.
- 516 Li, Q., Parrish, R., Horstwood, M., and McArthur, J.: U–Pb dating of cements in Mesozoic ammonites,
517 *Chemical Geology*, 376, 76-83, 2014.
- 518 MacDonald, J., Faithfull, J., Roberts, N., Davies, A., Holdsworth, C., Newton, M., Williamson, S.,
519 Boyce, A., John, C. J. C. t. M., and Petrology: Clumped-isotope palaeothermometry and LA-ICP-MS
520 U–Pb dating of lava-pile hydrothermal calcite veins, 174, 63, 2019.
- 521 Mason, A. J., Henderson, G. M., and Vaks, A.: An Acetic Acid-Based Extraction Protocol for the
522 Recovery of U, Th and Pb from Calcium Carbonates for U-(Th)-Pb Geochronology, *Geostandards and*
523 *Geoanalytical Research*, 37, 261-275, 10.1111/j.1751-908X.2013.00219.x, 2013.

- 524 Nuriel, P., Weinberger, R., Kylander-Clark, A. R. C., Hacker, B. R., and Craddock, J. P.: The onset of
525 the Dead Sea transform based on calcite age-strain analyses, *Geology*, 45, 587-590, 10.1130/g38903.1,
526 2017.
- 527 Nuriel, P., Craddock, J., Kylander-Clark, A. R., Uysal, I. T., Karabacak, V., Dirik, R. K., Hacker, B. R.,
528 and Weinberger, R. J. G.: Reactivation history of the North Anatolian fault zone based on calcite age-
529 strain analyses, 47, 465-469, 2019.
- 530 Parrish, R. R., Parrish, C. M., and Lasalle, S.: Vein calcite dating reveals Pyrenean orogen as cause of
531 Paleogene deformation in southern England, *Journal of the Geological Society*, 10.1144/jgs2017-107,
532 2018.
- 533 Piccione, G., Rasbury, E. T., Elliott, B. A., Kyle, J. R., Jaret, S. J., Acerbo, A. S., Lanzirotti, A.,
534 Northrup, P., Wootton, K., and Parrish, R. R.: Vein fluorite U-Pb dating demonstrates post-6.2 Ma rare-
535 earth element mobilization associated with Rio Grande rifting, *Geosphere*, 15, 1958-1972, 2019.
- 536 Ring, U., and Gerdes, A.: Kinematics of the Alpenrhein-Bodensee graben system in the Central Alps:
537 Oligocene/Miocene transtension due to formation of the Western Alps arc, *Tectonics*, 35, 1367-1391,
538 10.1002/2015TC004085/abstract, 2016.
- 539 Roberts, N. M., and Walker, R. J.: U-Pb geochronology of calcite-mineralized faults: Absolute timing
540 of rift-related fault events on the northeast Atlantic margin, *Geology*, 44, 531-534, 2016.
- 541 Roberts, N. M., Rasbury, E. T., Parrish, R. R., Smith, C. J., Horstwood, M. S., and Condon, D. J.: A
542 calcite reference material for LA-ICP-MS U-Pb geochronology, *Geochemistry, Geophysics, Geosystems*,
543 2017.
- 544 Roberts, N. M. W., Drost, K., Horstwood, M. S. A., Condon, D. J., Chew, D., Drake, H., Milodowski,
545 A. E., McLean, N. M., Smye, A. J., Walker, R. J., Haslam, R., Hodson, K., Imber, J., Beaudoin, N., and
546 Lee, J. K.: Laser ablation inductively coupled plasma mass spectrometry (LA-ICP-MS) U-Pb carbonate
547 geochronology: strategies, progress, and limitations, *Geochronology*, 2, 33-61, 10.5194/gchron-2-33-
548 2020, 2020.
- 549 Schmitz, M. D., and Schoene, B.: Derivation of isotope ratios, errors, and error correlations for U-Pb
550 geochronology using ^{205}Pb - ^{235}U -(^{233}U)-spiked isotope dilution thermal ionization mass
551 spectrometric data, *Geochemistry, Geophysics, Geosystems*, 8, 2007.
- 552 Vaks, A., Bar-Matthews, M., Matthews, A., Ayalon, A., and Frumkin, A.: Middle-Late Quaternary
553 paleoclimate of northern margins of the Saharan-Arabian Desert: reconstruction from speleothems of
554 Negev Desert, Israel, *Quaternary Science Reviews*, 29, 2647-2662, 2010.
- 555 Vaks, A., Woodhead, J., Bar-Matthews, M., Ayalon, A., Cliff, R. A., Zilberman, T., Matthews, A., and
556 Frumkin, A.: Pliocene-Pleistocene climate of the northern margin of Saharan-Arabian Desert recorded
557 in speleothems from the Negev Desert, Israel, *Earth and Planetary Science Letters*, 368, 88-100,
558 <http://dx.doi.org/10.1016/j.epsl.2013.02.027>, 2013.
- 559 van Elteren, J. T., Šelih, V. S., Šala, M., Van Malderen, S. J., and Vanhaecke, F.: Imaging artifacts in
560 continuous scanning 2D LA-ICPMS imaging due to nonsynchronization issues, *Analytical chemistry*,
561 90, 2896-2901, 2018.
- 562 van Elteren, J. T., Šelih, V. S., and Šala, M.: Insights into the selection of 2D LA-ICP-MS (multi)
563 elemental mapping conditions, *Journal of Analytical Atomic Spectrometry*, 34, 1919-1931, 2019.
- 564 van Malderen, S.: Optimization of methods based on laser ablation-ICP-mass spectrometry (LA-ICP-
565 MS) for 2-D and 3-D elemental mapping, Ghent University, 2017.

- 566 Vermeesch, P.: IsoplotR: A free and open toolbox for geochronology, *Geoscience Frontiers*, 2018.
- 567 von Quadt, A., Wotzlaw, J.-F., Buret, Y., Large, S. J., Peytcheva, I., and Trinquier, A.: High-precision
568 zircon U/Pb geochronology by ID-TIMS using new 10 13 ohm resistors, *Journal of Analytical Atomic*
569 *Spectrometry*, 31, 658-665, 2016.
- 570 Woodhead, J., and Petrus, J. J. G.: Exploring the advantages and limitations of in situ U–Pb carbonate
571 geochronology using speleothems, 1, 69-84, 2019.
- 572 Woodhead, J. D., and Hergt, J. M.: Strontium, neodymium and lead isotope analyses of NIST glass
573 certified reference materials: SRM 610, 612, 614, *Geostandards Newsletter*, 25, 261-266, 2001.
- 574 Wotzlaw, J.-F., Buret, Y., Large, S. J., Szymanowski, D., and von Quadt, A.: ID-TIMS U–Pb
575 geochronology at the 0.1‰ level using 10 13 Ω resistors and simultaneous U and 18 O/16 O isotope
576 ratio determination for accurate UO 2 interference correction, *Journal of Analytical Atomic*
577 *Spectrometry*, 32, 579-586, 2017.
- 578